Biochemical and Biophysical Research Communications 450 (2014) 390–395

Contents lists available at ScienceDirect

Biochemical and Biophysical Research Communications

journal homepage: www.elsevier.com/locate/ybbrc

Atomic resolution crystal structure of *Vc*LMWPTP-1 from *Vibrio cholerae* O395: Insights into a novel mode of dimerization in the low molecular weight protein tyrosine phosphatase family ☆

Seema Nath, Ramanuj Banerjee, Udayaditya Sen *

Crystallography and Molecular Biology Division, Saha Institute of Nuclear Physics, 1/AF, Bidhannagar, Kolkata 700064, India

ARTICLE INFO

Article history:
Received 19 May 2014
Available online 6 June 2014

Keywords:
Bacterial protein phosphatases
Low molecular weight protein tyrosine phosphatases
X-ray crystallography
Active dimer

ABSTRACT

Low molecular weight protein tyrosine phosphatase (LMWPTP) is a group of phosphotyrosine phosphatase ubiquitously found in a wide range of organisms ranging from bacteria to mammals. Dimerization in the LMWPTP family has been reported earlier which follows a common mechanism involving active site residues leading to an enzymatically inactive species. Here we report a novel form of dimerization in a LMWPTP from *Vibrio cholera* 0395 (*Vc*LMWPTP-1). Studies in solution reveal the existence of the dimer in solution while kinetic study depicts the active form of the enzyme. This indicates that the mode of dimerization in *Vc*LMWPTP-1 is different from others where active site residues are not involved in the process. A high resolution (1.45 Å) crystal structure of *Vc*LMWPTP-1 confirms a different mode of dimerization where the active site is catalytically accessible as evident by a tightly bound substrate mimicking ligand, MOPS at the active site pocket. Although being a member of a prokaryotic protein family, *Vc*LMWPTP-1 structure resembles very closely to LMWPTP from a eukaryote, *Entamoeba histolytica*. It also delineates the diverse surface properties around the active site of the enzyme.

1. Introduction

Reversible protein phosphorylation is an important event involved in intracellular signal transduction pathways in response to triggering factors which regulate crucial metabolic activities in cell. The net result of incorporation of phosphate groups in proteins is diverse and this probably acts as a key step in cellular regulation [1]. The overall content of phosphotyrosine in cells is reciprocally controlled by protein tyrosine kinases (PTKs) which specifically phosphorylate tyrosines in proteins [2]. An abundant member of this class of proteins is the low molecular weight protein tyrosine phosphatases (LMWPTPs) ubiquitously found in all organisms ranging from prokaryotes to higher eukaryotes. LMWPTPs belong to class II PTPs which act on tyrosine phosphorylated proteins, low molecular weight aryl phosphates and natural and synthetic acyl phosphates [3].

Several structures of LMWPTP from eukaryotic organism such as human – HCPTPA (PDB: 5PNT) [4], bovine – BPTPA (PDB: 1Z12) [5], mouse – RPTPA (PDB: 2P4U) [6], yeast – LTP1 (PDB: 1D1P) [7] and protozoan parasite *Entamoeba histolytica* – EhPtp (PDB: 3IDO) [8] are available. From the prokaryotic counterpart, structures of LMWPTP from gram-positive eubacteria *Staphylococcus aureus* – PtpA (PDB: 3ROF) [9], gram-negative eubacteria *Thermus thermophilus* – TT1001 (PDB: 2CWD), gram-positive proteobacteria *Bacillus subtilis* – YwlE (PDB: 4ETI) [10], gram-negative proteobacteria *Escherichia coli* – Wzb (PDB: 2WJA) and pathogenic *Mycobacterium tuberculosis* MPtpA (PDB: 1U2Q) [11] are available. It has been reported that the self association of mammalian LMWPTP (viz. *Bos taurus* LMWPTP, BPTP) produces inactive oligomers that are in equilibrium with its active monomers [12]. Among the prokaryotic LMWPTPs weak oligomerization has been found to exist in YwlE from *B. subtilis*, PtpB from the Gram-negative bacterium *Salmonella aureus* and *E. coli* Wzb. However the mode of dimerization is similar in both the cases and takes place through the direct involvements of the active site residues and the tyrosines of the DPY-loop, leading to a catalytically inactive species [13].

Here we report a novel mode of dimerization of *Vc*LMWPTP-1, a 17.9 kDa (155 amino acids) protein from *Vibrio cholerae* O395. Fast protein liquid chromatography and glutaraldehyde crosslinking

Abbreviations: LMWPTP, low molecular weight protein tyrosine phosphatases; FPLC, fast protein liquid chromatography; MOPS, 3-(N-morpholino) propanesulfonic acid.

☆ Protein Data Bank: Coordinates and structure factor files have been deposited with the accession code 4LRQ.

* Corresponding author. Fax: +91 33 2337 4637.
E-mail address: udayaditya.sen@saha.ac.in (U. Sen).

http://dx.doi.org/10.1016/j.bbrc.2014.05.129
0006-291X/

reveal the existence of the dimeric species of the protein in solution. Kinetic studies of *Vc*LMWPTP-1 using para-nitro phenyl phosphate (pNPP) as the substrate depicts that the protein is active, suggesting that the mode of dimerization in *Vc*LMWPTP-1 is different from other LMWPTPs. In an attempt to investigate the molecular mechanism of this form of dimerization, we solved a high resolution crystal structure (1.45 Å) of *Vc*LMWPTP-1 which depicts a mode of dimerization markedly different from those reported for other dimeric LMWPTPs. The extensive dimerization interface area of *Vc*LMWPTP-1 is about double than that of other mode of dimerization and active site residues are not seen to be involved in the oligomerization. The active site of each monomer is totally accessible to the substrate which is evident from the crystal structure where the active site of each monomer is occupied by a tightly bound MOPS molecule in a substrate like manner. Comparison of the *Vc*LMWPTP-1 structure and surface properties with similar structures in the PDB illuminates its structural convergence with LMWPTP from a eukaryote, *E. histolytica*.

2. Materials and methods

2.1. Cloning, expression and purification

*Vc*LMWPTP-1 protein was cloned, over expressed and purified as mentioned earlier [14]. Active site mutant of *Vc*LMWPTP-1, C8S was cloned using two-step PCR method and inserted after the start codon of pET24b(+). The mutant was overexpressed as C-terminal His-tag and was purified in similar way of the wild type.

2.2. Determination of oligomers using FPLC

*Vc*LMWPTP-1 (0.85 mg/ml, 1.75 mg/ml, 2.58 mg/ml and 4.25 mg/ml) in three different 50 mM Tris buffer, each at pH 7.6 containing 150 mM, 300 mM and 500 mM NaCl was fractionated by a Sephacryl S-100 (Amersham Biosciences) column (46 × 1.6 cm) at 0.9 MPa, pre-equilibrated with respective buffers and precalibrated with a protein mixture containing Lysozyme (MW14.3 kDa) Ovalbumin (MW 36.0 kDa) and Bovine serum albumin (MW 66.45 kDa) at room temperature. Fractions were collected at a flow rate of 0.4 ml per minute using an ÄKTAPrime chromatographic system. The elution profile was determined by monitoring the absorbance at 280 nm.

2.3. Crystallization, data collection and structure solution

Crystallization and data collection of *Vc*LMWPTP-1 was reported earlier [14].For phasing the 1.45 Å data of the crystal, the coordinates of *E. histolytica* (PDB: 3IDO) [8] was used for molecular replacement with Phaser [15] in CCP4 [16] with V_m of 2.18 (solvent content 43.63%), final TFZ = 13.3 and LLG = 157. Model building was done with Coot [17] and refinement was carried out with Phenix refine [18] with twin law -k,-h,-l. TLS refinement was performed during the final stages of refinement [19].

2.4. Structural analysis

Average B-factors for each residue were calculated using B average in CCP4 [20]. PISA webserver [21] and PIC server [22] were used for analysis of the structure and oligomeric state. The oligomeric state and other structural of the protein was analyzed using the. Sequence alignment of *Vc*LMWPTP-1 with other lmwptps was done using ClustalO [23,24]. Figures were prepared using Pymol (http://www.pymol.org). The surface electrostatic potential was mapped using Chimera [25] [−10 kT/e (red) to +10 kT/e (blue)].

2.5. Enzyme kinetics

Kinetic parameters were calculated for *Vc*LMWPTP-1 using *p*-nitrophenyl phosphate (pNPP) as the substrate as described [26]. Briefly, pNPP at a concentration range of 1–40 mM was treated with 100 μM *Vc*LMWPTP-1 and C8S mutant and quenched with 1 N NaOH after 10 min. The absorbance of the product, *p*-nitrophenol, thus formed is measured at 405 nm. The amount of *p*-nitrophenol was calculated from the standard curve of *p*-nitrophenol. For standard curve, stock solution of *p*-nitrophenol was diluted with 0.05 N NaOH and the absorbance of the samples was measured at 405 nm. To check the effect of temperature on the enzymatic activity samples were incubated at 5 °C interval in the water-bath prior to check the absorbance.

2.6. Glutaraldehyde crosslinking to capture the dimeric state in solution

For crosslinking assays, 2.3% freshly prepared solution of glutaraldehyde was added to a reaction mixture of 100 μl containing about 50 μg of the protein in 50 mM MOPS, pH 7.6, 300 mM NaCl and the reaction carried out at room temperature (25 °C). Samples were collected at 15 s, 30 s, 1 min and then up to 5 min at an interval of 1 min and quenched by addition of 10 μl of 1 M Tris–HCl, pH 8.0. Cross-linked proteins were analyzed through 15% SDS–PAGE.

3. Results and discussion

3.1. VcLMWPTP-1 forms dimer in solution

*Vc*LMWPTP-1 elutes as a single peak in fast protein liquid chromatography (FPLC) (Fig. 1A) and calculations based upon standard curve shows that this species is the dimeric form of *Vc*LMWPTP-1 (Fig.1B and C). Moreover, presence of the dimeric form is observed irrespective of protein or salt (NaCl) concentration. Further confirmation of the dimeric form was performed through glutaraldehyde crosslinking where a gradual increase in the dimeric band with time could be seen in 15% SDS–PAGE (Fig. 1F).

3.2. Phosphatase activity of VcLMWPTP-1

Enzyme kinetic assays for *Vc*LMWPTP-1 were performed at pH 4.8 and pH 7.6 at 25 °C using *p* nitrophenyl phosphate as a substrate (Materials and Methods). The determined K_m value under these conditions was 2.07 ± 0.2 mM and 2.03 ± 0.4 mM respectively (Fig. 1D), which is consistent with the K_m values reported for other LMWPTPs like PtpA and PtpB (1.2 and 1.5 mM) [27]. This leads us to propose that the respective active site of the dimer is accessible to the substrate. So the dimer formed in case of *Vc*LMWPTP-1 does not involve active site residues as commonly found in previously reported inactive dimeric species of LMWPTPs and pH variation has no effect on its catalytic activity. The enzyme shows optimum activity at 25 °C and the activity decreases with increasing temperature leading to complete loss of activity at 55 °C (Fig. 1E). Mutating the active site Cys8 to Ser (C8S) results in complete loss of enzymatic activity (Fig. 1E inset) as reported for other LMWPTPS [28].

3.3. Overall structure of VcLMWPTP-1 monomer

*Vc*LMWPTP-1 crystallized in space group $P3_1$ using ammonium sulfate (AMS) as precipitant and the structure has been solved at 1.45 Å (Supplementary Table S1). The asymmetric unit contains four molecules of *Vc*LMWPTP-1 and their arrangement suggests that molecules A and C and molecules B and D assemble together

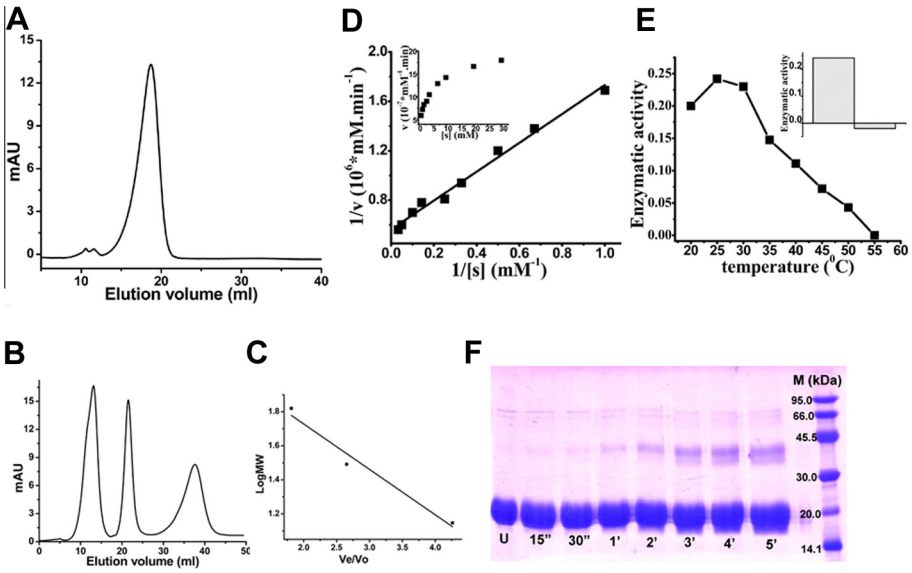

Fig. 1. Existence of oligomeric *Vc*LMWPTP-1 in solution and its activity. (A) FPLC analysis of *Vc*LMWPTP-1. The elution volume of the peak-2 corresponds to a dimeric *Vc*LMWPTP-1 species, peak-1 is impurity. (B) Calibration of the column using a mixture of proteins (peak 1-Lysozyme, MW14.3 kDa; peak 2-ovalbumin, MW 36.0 kDa and peak 3-Bovine serum albumin, MW 66.45 kDa) and (C) the standard curve is drawn based on the elution profile of protein mixtures of known molecular weights. (D) V/[S] graph of *Vc*LMWPTP-1 (inset), Double Reciprocal plot of *Vc*LMWPTP-1 at pH 4.8. (E) Enzymatic activity (μmoles min^{-1} $μg^{-1}$) of *Vc*LMWPTP-1 with temperature (°C); optimum enzymatic activity is observed at 25 °C while complete loss of activity occurs at 55 °C. Comparative enzymatic activity of *Vc*LMWPTP-1 and C8S mutant (inset) at 25 °C demonstrating that Cys to Ser mutation at the active site results in the complete loss of catalytic activity. (F) 15% SDS–PAGE profile of Glutaraldehyde crosslinked *Vc*LMWPTP-1 showing a gradual increase in the dimeric species (~40 kDa) with time. Lane 1: untreated protein, lane 2–8: glutaraldehyde treated protein, lane 10: protein marker. The band corresponding to the dimeric *Vc*LMWPTP-1 becomes prominent from 1 min between 45.0 and 30.0 kDa.

to form two dimers. The high resolution electron density map allowed us to locate 149 residues out of 155 residues of each *Vc*LMWPTP-1 molecule. Each *Vc*LMWPTP-1 binds a MOPS molecule in its active site and one sulfate at the C-terminal loop. The fold and overall secondary structure is comprised of three layer βαβ sandwiched architecture with a topology of Rossmann fold and the four stranded parallel β-sheet is sandwiched between three long (α1, α4 and α6) and three short (α2, α3, α5) helices (Fig. 2A).

3.4. Ligand bound 'closed structure' conformation

The active site is located at the crevice formed by loop-1 between β1 and α1, also called P-loop. It is surrounded by long, flexible loop-3 and short loop-6 and the DPY-loop, which is a portion of loop-8 preceding the last helix (α6) that contributes residue (D122) necessary for the catalytic action (Fig. 2A). From the well defined electron density it was evident that each *Vc*LMWPTP-1 molecule tightly binds a ligand molecule, MOPS at the active site. Main-chain amide nitrogens of the residues constituting the P-loop and the side-chain amide nitrogens of Arg14 are engaged in the binding and stabilization of the sulfonate group of the ligand (Fig. 2B). A stereo representation of the electron density map around the active site of *Vc*LMWPTP-1 molecule is shown in Supplementary Fig. S1. The piperazine ring of MOPS molecule is surrounded with several polar and aromatic residues (Thr40, Tyr43, His44, Asn47, Asp87, Glu89, Asn90, Asp122, Tyr124, and Tyr125) and they define the architecture of the wall of the deep phosphotyrosine binding pocket of *Vc*LMWPTP-1 with an opening at one side (Fig. 2C). The ligand mimics the substrate phosphotyrosine as seen in PTP1B (PDB: 1G1F) [29] (Fig. 2D). The catalytic S^{γ} of Cys8 point towards the S1-atom of MOPS (that corresponds to the P atom of Phosphotyrosine) at a distance of 3.8 Å and is in a position to accept the phosphoryl group. Asp122 of DPY-loop comes close to the P-loop after MOPS binding and its side-chain oxygen atoms are within 3.4 Å with the C1 atom of the MOPS molecule (that corresponds to the phenolate O atom of the Phosphotyrosine). At this distance Asp122 serves as an acid catalyst for the leaving alcoholic group. The covering of MOPS molecule with Thr40, Tyr43, His44, Asn47, Asp87, Glu89, Asn90, Asp122, Tyr124,Tyr125 and the disposition of catalytic Cys8 and Asp122 near the leaving group together resembles a substrate bound 'closed structure'. This closure at the P-loop pocket is also evident from the structural alignment with an 'open structure' of apo-MPtpA (PDB: 2LUO) [30] to the ligand-bound structures (PDB: 1U2P, 1U2Q) [11] where the position of DPY-loop is shown to be closer to P-loop in case of the ligand-bound structure than the apo-form [30].

3.5. Multiple sequence alignment showing conserved motifs

Multiple sequence alignment and 3D superposition of LMWPTP structures determined from other organisms show that their active site is highly conserved (Supplementary Fig. S2). Among these structures *Vc*LMWPTP-1 shares highest sequence identity (43%) with that of *E. histolytica* (PDB: 3JVI) [8] with an average RMSD of superposition 0.48 Å for 122 residues. Structural superposition indicates that the end of the distorted α4 and region preceding the catalytically important DPY-loop exhibits highest variability. Comparison of the structure of *Vc*LMWPTP-1 to PtpA, LMWPTP from gram-positive eubacteria *Staphylococcus aureus* (PDB: 3ROF) [9]; YwlE, LMWPTP from gram-positive proteobacteria *B. subtilis* (PDB: 4ETI) and Wzb, LMWPTP from gram-negative proteobacteria *E. coli* (PDB: 2WJA) [10] also indicates significant structural difference around loop-3 which is closer to the P-loop. Besides the active site P-loop and DPY-loop, two more conserved sequences (motif) are evident from the alignment result. Details of the four motifs and possible role of the conserved residues are listed in Supplementary Table S2. The active site structure of PTPs follow the active site motif of CX_5R, the only common feature between the large PTP family and LMWPTP [31]. Sequence alignment helps to dissect the

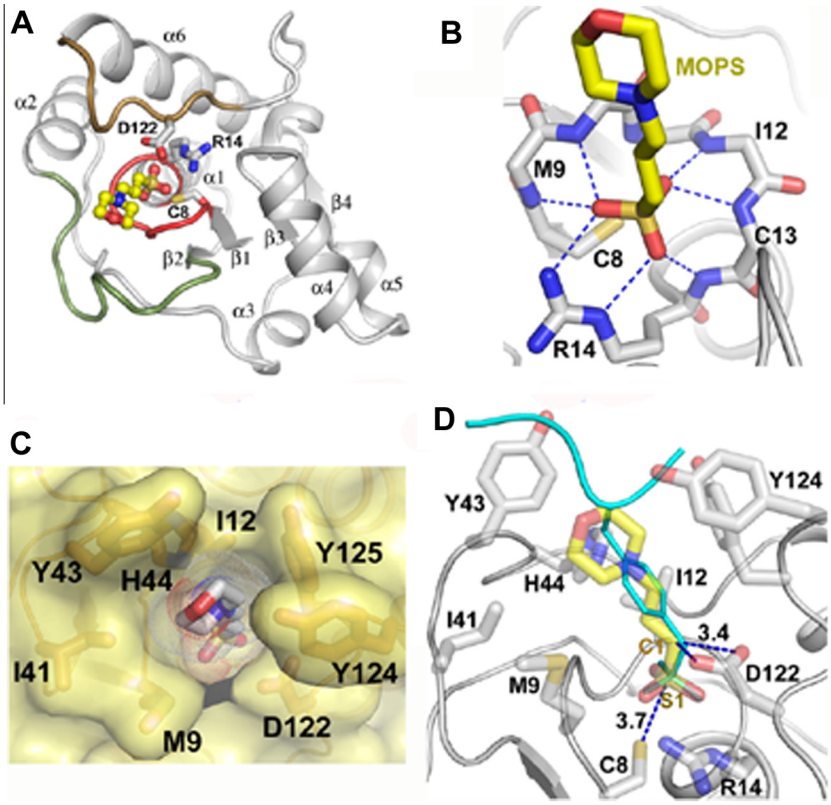

Fig. 2. Overall structure and MOPS binding at the active site of *Vc*LMWPTP-1. (A) Cartoon representation of the secondary structure of *Vc*LMWPTP-1 monomer. The MOPS molecule (ball and sticks) at active site where residues C8, R14 in red colored P-loop, D122 in brown colored DPY loop and loop α2-β2 (olive) responsible for catalytic action. (B) Extensive hydrogen bonds made by the sulfonyl group of the MOPS molecule with the amide environment of the P-loop and the side chain of R14. (C) Surface representation of *Vc*LMWPTP-1 depicting the residues defining the active site pocket (surface and stick) that tightly bind the MOPS molecule (dots and stick). (D) Similarity of binding of MOPS with that of phosphotyrosine (cyan) (PDB: 1XXV) binding. The residues of *Vc*LMWPTP-1 that define the active site along with the MOPS molecule are shown as transparent sticks while the side chain of nonhydrolyzable phosphotyrosine in thick lines (cyan). The position of sulfonyl group of the MOPS molecule (stick) is almost indistinguishable with the phosphate group of phosphotyrosine. Distance between S^{γ} atom of Cys8 and the S1 atom of MOPS (that corresponds the P atom of phosphotyrosine) is 3.7 Å, capable to accept the phosphoryl group. Distance between OD1 (or OD2) of D122 and C1 of MOPS (that corresponds the OH atom of phosphotyrosine) is 3.4 Å and in a position to serve as an acid catalyst. (For interpretation of the references to color in this figure legend, the reader is referred to the web version of this article.)

'X_5' portion of the P-loop sequence revealing '(T/L/M)GN(I/L)C' as a consensus motif in this family, contrary to the notion of being tagged as 'any amino acid'. It is also to be noted that the flanking residue(s) beside the P-loop is hydrophobic in nature. Motif-1 and Motif-4 are parts of P-loop and DPY-loop respectively. Motif-2 containing loop-2 is in close proximity to the active site whereas Motif-3 containing β3 is remotely distant from the active site. Motif-2 region superposes well in 3D structures between *Vc*LMWPTP-1 with eukaryotic LMWPTPs but a marked distortion with the prokaryotic counterpart is evident, especially with Wzb, YwlE and PtpA.

3.6. Dimerization of VcLMWPTP-1: role of a set of unique residues

Crystal structure of *Vc*LMWPTP-1 shows that each dimer (A:C and B:D) faces an extended surface area that is further stitched by two sulfate ions at the interfacial region (Fig. 3A). Calculation of buried surface area (BSA) by PISA [21] shows 2910 $Å^2$ BSA for the B:D dimer and 2820 $Å^2$ BSA for the A:C dimer. The BSA of both the dimers is ~20% of their respective accessible surface area (ASA) and ~10% of their total ASA. PISA server also indicates that the average ΔG_{diss} value of both the dimers is ~14 kcal.mol^{-1} indicating they are stable in solution. At the interfacial region, twelve residues (Met9, Thr40, Ile41, Gly42, Tyr43, Lys71, Glu89, Ala92, Glu93, Arg97, Tyr124, and Tyr125) play pivotal role to stabilize the dimers through numerous hydrophobic and H-bonding interactions (Fig. 3B). Tyr43 and Lys71 from each chain are involved in cation-TT interaction with its dimeric counterpart. Sulfate ions which stitch the two monomers interacts with the main chain NH of Gly42 and the side chain NZ of Lys71 of one monomer and the main chain NH of Tyr43 of the other monomer. In contrast to the buried surface area (BSA) of *Vc*LMWPTP-1 (average BSA 2865 $Å^2$) the dimerization region of BPTP encompasses a much smaller BSA (1589 $Å^2$) that consist only the residues from the active site and DPY-loop (Fig. 3C and D).

Analysis of the position of Lys residues at the dimeric interface of the *Vc*LMWPTP-1 (Fig. 3E) shows only a pair of amine (Lys68 from each monomer at a distance of ~10 Å) which could crosslink with each other in presence of glutaraldehyde (Fig. 3E). Distance between all other inter-monomeric Lys residues and the N terminus amines are beyond the condensable distance. As this mode of dimerization is stabilized by hydrophobic and polar interactions, it would show a monomeric band in SDS–PAGE. However, if the dimer is crosslinked by glutaraldehyde a band near its dimer appears with time. Since the distance between Lys68 in the dimer is little larger than the condensable distance (6–8 Å), more dimers become crosslinked with gradual increase in time (Fig. 1F).

3.7. Insight into substrate specificity – diverged surface property around the active site

CASTp server [32] shows 256 $Å^3$ as the volume of the active site cavity. Comparison of the structure and electrostatic surface around the active site of *Vc*LMWPTP-1 with others reveals

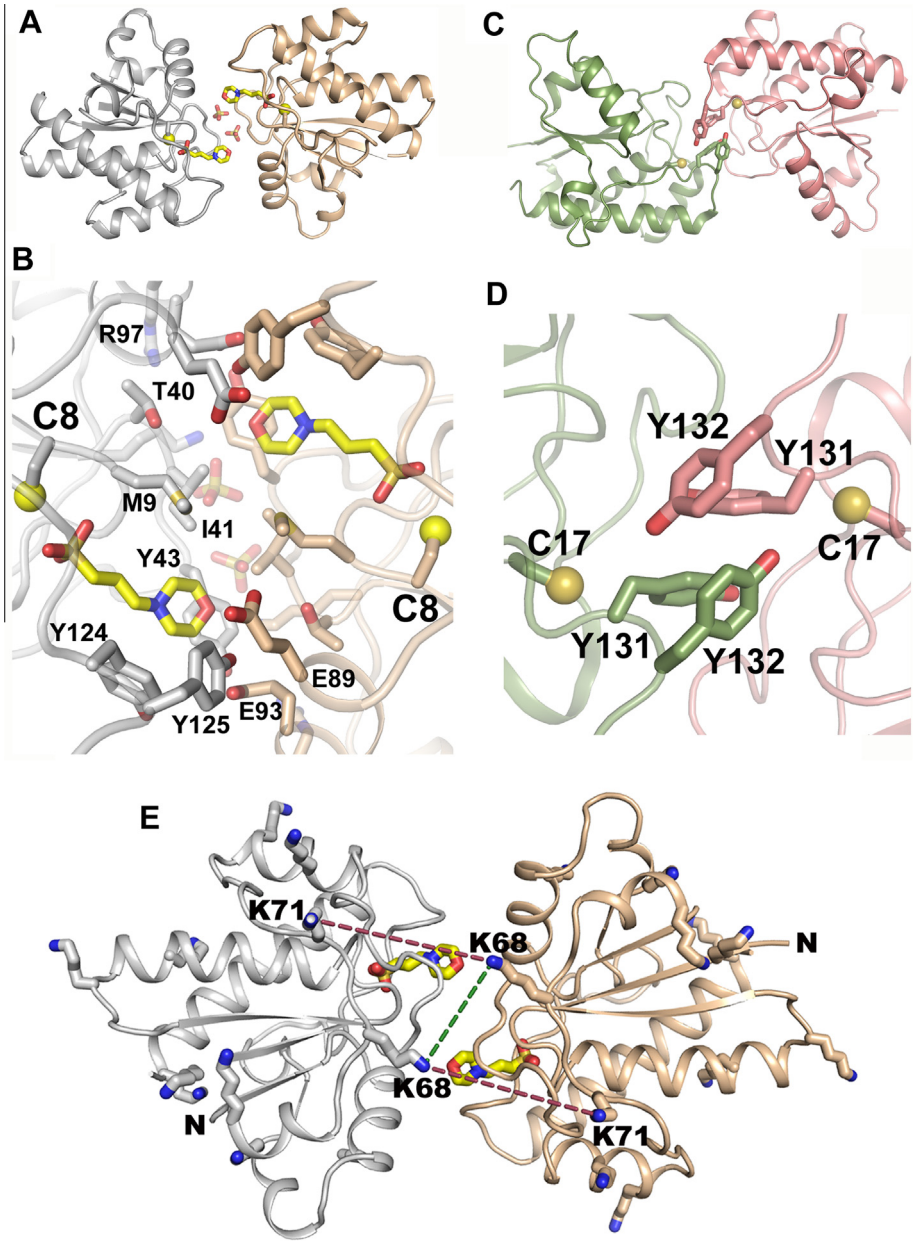

Fig. 3. Comparison of dimeric interface of *Vc*LMWPTP-1 (left) with that of bovine LMWPTPs (BPTP) (right). (A) Cartoon representation of the *Vc*LMWPTP-1 dimer (gray and wheat) with the bound MOPS molecule (yellow) and sulfate ions (in sticks). (B) Close-up view of the dimeric interface of *Vc*LMWPTP-1 highlighting the residues involved in dimerization. Y124 and Y125 of the DPY loop are engaged in dimerization but keep the catalytic pocket accessible. (C) Cartoon representation of the BPTP dimer (green and salmon). (D) Close-up view showing Y131, Y132 of the DPY loop of one molecule comes in close proximity to the active site of the other molecule resulting in the inactivation of the enzymes. (E) Dimeric structure of *Vc*LMWPTP-1 and amine residues (Lysine and N-terminus residues) that may react with glutaraldehyde. The smallest distance is 10 Å (shown in green dashed line) between K68 from each monomer that can cross-link with each other while the next larger distance is 17 Å (red dashed line) which is beyond the cross-linking range of glutaraldehyde. (For interpretation of the references to color in this figure legend, the reader is referred to the web version of this article.)

close resemblance with EhPtp and other mammalian LMWPTPs than with LMWPTPs of bacterial origin (Supplementary Fig. S3). *Vc*LMWPTP-1 differs with prokaryotic LMWPTPs at two regions which are implicated in substrate recognition and binding. The W-loop, harboring a Trp-residue almost in every LMWPTP, is proposed to play an important role in substrate recognition [10]. However, corresponding residue is Tyr43 in *Vc*LMWPTP-1 and Tyr49 in HCPTPA, important for substrate recognition for the latter. But in bacteria, Tyr43 is substituted by Leu44 in Wzb and Ser42 in YwlE. Asn53 in HCPTPA plays a crucial role in determining the substrate specificity [3], corresponding residue Asn47 in *Vc*LMWPTP-1 may play a similar role. Again this is in sharp contrast with bacterial LMWPTPs like Wzb, Ptp where the corresponding residue K43 and Y44 respectively play indispensable role in substrate recognition [10]. Overall, these differences from prokaryotic LMWPTPs make *Vc*LMWPTP-1 active site more like eukaryotic than of prokaryotic origin which may dictate its substrate specificity.

In conclusion, we report an exclusive dimeric species of *Vc*LMWPTP-1 in solution through FPLC while atomic resolution X-ray structure shows that the dimeric species is 'novel' where the active site is not occluded. This dimer is catalytically active as demonstrated by kinetic studies while a MOPS molecule bound in a substrate like manner at the active site proves the active pocket is accessible for the substrate. *Vc*LMWPTP-1 also distinguishes itself

from other bacterial LMWPTPs in terms of electrostatic charge distribution around the active site thereby suggesting close similarity in substrate(s) preference to eukaryotic LMWPTPs, than its bacterial homologue. Since the dimeric surface is closer to the active site it may further modulate the substrate recognition and specificity.

Acknowledgments

The laboratory of US is partly supported by the MSACR project, DAE, Govt. of India, SINP. RB is a Senior Research Fellow of the Council of Scientific and Industrial Research, India. SN is a Senior Research Fellow of the Department of Atomic Energy, India. US thank Dr. J. Dasgupta for her help during FPLC experiments.

Appendix A. Supplementary data

Supplementary data associated with this article can be found, in the online version, at http://dx.doi.org/10.1016/j.bbrc.2014.05.129.

References

[1] L.N. Johnson, The regulation of protein phosphorylation, Biochem. Soc. Trans. 37 (2009) 627–641.
[2] T. Mustelin, K. Taskén, Positive and negative regulation of T-cell activation through kinases and phosphatases, Biochem. J. 371 (2003) 15–27.
[3] Y.Y. Wo, A.L. McCormack, J. Shabanowitz, D.F. Hunt, J.P. Davis, G.L. Mitchell, R.L. Van Etten, Sequencing, cloning, and expression of human red cell-type acid phosphatase, a cytoplasmic phosphotyrosyl protein phosphatase, J. Biol. Chem. 267 (1992) 10856–10865.
[4] M. Zhang, C.V. Stauffacher, D. Lin, R.L. Van Etten, Crystal structure of a human low molecular weight phosphotyrosyl phosphatase. Implications for substrate specificity, J. Biol. Chem. 273 (1998) 21714–21720.
[5] M. Zhang, M. Zhou, R.L. Van Etten, C.V. Stauffacher, Crystal structure of bovine low molecular weight phosphotyrosyl phosphatase complexed with the transition state analog vanadate, Biochemistry 36 (1997) 15–23.
[6] S.C. Almo, J.B. Bonanno, J.M. Sauder, S. Emtage, T.P. Dilorenzo, V. Malashkevich, S.R. Wasserman, S. Swaminathan, S. Eswaramoorthy, R. Agarwal, D. Kumaran, M. Madegowda, S. Ragumani, Y. Patskovsky, J. Alvarado, U.A. Ramagopal, J. Faber-Barata, M.R. Chance, A. Sali, A. Fiser, Z.Y. Zhang, D.S. Lawrence, S.K. Burley, Structural genomics of protein phosphatases, J. Struct. Funct. Genomics 8 (2007) 121–140.
[7] S. Wang, L. Tabernero, M. Zhang, E. Harms, R.L. Van Etten, C.V. Stauffacher, Crystal structures of a low-molecular weight protein tyrosine phosphatase from *Saccharomyces cerevisiae* and its complex with the substrate *p*-nitrophenyl phosphate, Biochemistry 39 (2000) 1903–1914.
[8] A.S. Linford, N.M. Jiang, T.E. Edwards, N.E. Sherman, W.C. Van Voorhis, L.J. Stewart, P.J. Myler, B.L. Staker, W.A. Petri Jr., Crystal structure and putative substrate identification for the *Entamoeba histolytica* low molecular weight tyrosine phosphatase, Mol. Biochem. Parasitol. 193 (2014) 33–44.
[9] C. Vega, S. Chou, K. Engel, M.E. Harrell, L. Rajagopal, C. Grundner, Structure and substrate recognition of the *Staphylococcus aureus* protein tyrosine phosphatase PtpA, J. Mol. Biol. 413 (2011) 24–31.
[10] G. Hagelueken, H. Huang, I.L. Mainprize, C. Whitfield, J.H. Naismith, Crystal structures of Wzb of *Escherichia coli* and CpsB of *Streptococcus pneumoniae*, representatives of two families of tyrosine phosphatases that regulate capsule assembly, J. Mol. Biol. 392 (2009) 678–688.
[11] C. Madhurantakam, E. Rajakumara, P.A. Mazumdar, B. Saha, D. Mitra, H.G. Wiker, R. Sankaranarayanan, A.K. Das, Crystal structure of low-molecular-weight protein tyrosine phosphatase from *Mycobacterium tuberculosis* at 1.9-A resolution, J. Bacteriol. 187 (2005) 2175–2181.
[12] L. Tabernero, B.N. Evans, P.A. Tishmack, R.L. Van Etten, C.V. Stauffacher, The structure of the bovine protein tyrosine phosphatase dimer reveals a potential self-regulation mechanism, Biochemistry 38 (1999) 11651–11658.
[13] J. Blobel, P. Bernadó, H. Xu, C. Jin, M. Pons, Weak oligomerization of low-molecular-weight protein tyrosine phosphatase is conserved from mammals to bacteria, FEBS J. 276 (2009) 4346–4357.
[14] S. Nath, R. Banerjee, S. Khamrui, U. Sen, Cloning, purification, crystallization and preliminary X-ray analysis of two low-molecular-weight protein tyrosine phosphatases from *Vibrio cholerae*, Acta Crystallogr. Sect. F Struct. Biol. Cryst. Commun. 68 (2012) 1204–1208.
[15] A.J. McCoy, R.W. Grosse-Kunstleve, P.D. Adams, M.D. Winn, L.C. Storoni, R.J. Read, Phaser crystallographic software, J. Appl. Crystallogr. 40 (2007) 658–674.
[16] E. Potterton, P. Briggs, M. Turkenburg, E. Dodson, A graphical user interface to the CCP4 program suite, Acta Crystallogr. D Biol. Crystallogr. 59 (2003) 1131–1137.
[17] P. Emsley, K. Cowtan, Coot: model-building tools for molecular graphics, Acta Crystallogr. D Biol. Crystallogr. 60 (2004) 2126–2132.
[18] P.D. Adams, P.V. Afonine, G. Bunkóczi, V.B. Chen, I.W. Davis, N. Echols, J.J. Headd, L. Hung, G.J. Kapral, R.W. Grosse-Kunstleve, A.J. McCoy, N.W. Moriarty, R. Oeffner, R.J. Read, D.C. Richardson, J.S. Richardson, T.C. Terwilliger, P.H. Zwart, PHENIX: a comprehensive python-based system for macromolecular structure solution, Acta Crystallogr. D Biol. Crystallogr. 66 (2010) 213–221.
[19] J. Painter, E.A. Merritt, TLSMD web server for the generation of multi-group TLS models, J. Appl. Crystallogr. 39 (2006) 109–111.
[20] M.D. Winn, C.C. Ballard, K.D. Cowtan, E.J. Dodson, P. Emsley, P.R. Evans, R.M. Keegan, E.B. Krissinel, A.G. Leslie, A. McCoy, S.J. McNicholas, G.N. Murshudov, N.S. Pannu, E.A. Potterton, H.R. Powell, R.J. Read, A. Vagin, K.S. Wilson, Overview of theCCP4suite and current developments, Acta. Crystallogr. D 67 (2011) 235–242.
[21] E. Krissinel, K. Hendrick, Inference of macromolecular assemblies from crystalline state, J. Mol. Biol. 372 (2007) 774–797 and PISA web server: <http://www.ebi.ac.uk/msd-srv/prot_int/cgi-bin/piserver>.
[22] K.G. Tina, R. Bhadra, N. Srinivasan, PIC: protein interactions calculator, Nucleic Acids Res. 35 (2007) W473–W476.
[23] F. Sievers, A. Wilm, D.G. Dineen, T.J. Gibson, K. Karplus, W. Li, R. Lopez, H. McWilliam, M. Remmert, J. Söding, J.D. Thompson, D. Higgins, Fast, scalable generation of high-quality protein multiple sequence alignments using Clustal Omega, Mol. Syst. Biol. 11 (2011) 539.
[24] M. Goujon, H. McWilliam, W. Li, F. Valentin, S. Squizzato, J. Paern, R. Lopez, A new bioinformatics analysis tools framework at EMBL-EBI, Nucleic Acids Res. 38 (2010) W695–W699.
[25] E.F. Pettersen, T.D. Goddard, C.C. Huang, G.S. Couch, D.M. Greenblatt, E.C. Meng, T.E. Ferrin, UCSF Chimera – a visualization system for exploratory research and analysis, J. Comput. Chem. 25 (2004) 1605–1612.
[26] Z.Y. Zhang, R.L. Van Etten, Purification and characterization of a low-molecular-weight acid phosphatase – a phosphotyrosyl-protein phosphatase from bovine heart, Arch. Biochem. Biophys. 282 (1990) 39–49.
[27] D. Soulat, E. Vaganay, B. Duclos, A.L. Genestier, J. Etienne, A.J. Cozzone, *Staphylococcus aureus* contains two low-molecular-mass phosphotyrosine protein phosphatases, J. Bacteriol. 184 (2002) 5194–5199.
[28] J.P. Davis, M.M. Zhou, R.L. Van Etten, Kinetic and site-directed mutagenesis studies of the cysteine residues of bovine low molecular weight phosphotyrosyl protein phosphatase, J. Biol. Chem. 269 (1994) 8734–8740.
[29] A. Salmeen, J.N. Andersen, M.P. Myers, N.K. Tonks, D. Barford, Molecular basis for the dephosphorylation of the activation segment of the insulin receptor by protein tyrosine phosphatase 1B, Mol. Cell 6 (2000) 1401–1412.
[30] T. Stehle, S. Sreeramulu, F. Löhr, C. Richter, K. Saxena, H.R. Jonker, H. Schwalbe, The apo-structure of the low molecular weight protein-tyrosine phosphatase A (MptpA) from *Mycobacterium tuberculosis* allows for better target-specific drug development, J. Biol. Chem. 287 (2012) 34569–34582.
[31] E.B. Fauman, M.A. Saper, Structure and function of the protein tyrosine phosphatases, Trends Biochem. Sci. 21 (1996) 413–417.
[32] J. Dundas, Z. Ouyang, J. Tseng, A. Binkowski, Y. Turpaz, J. Liang, CASTp: computed atlas of surface topography of proteins with structural and topographical mapping of functionally annotated residues, Nucleic Acids Res. 1 (2006) 34.